Vietnam Journal of Earth Sciences, 43(4), 465-484, https://doi.org/10.15625/2615-9783/16502

Vietnam Academy of Science and Technology
Vietnam Journal of Earth Sciences
http://www.vjs.ac.vn/index.php/jse

Characterization of ionospheric irregularities over Vietnam and adjacent region for the 2008-2018 period

Dung Nguyen Thanh[1,2], Minh Le Huy[*1,2], Christine Amory-Mazaudier[3,4], Rolland Fleury[5], Susumu Saito[6], Thang Nguyen Chien[1], Hong Pham Thi Thu[1,2], Thanh Le Truong[1], Mai Nguyen Thi[1]

[1]*Institute of Geophysics, VAST, Hanoi, Vietnam*
[2]*Graduate University of Science and Technology, VAST, Hanoi, Vietnam*
[3]*Sorbonne Universités, UPMC Univ. Paris 06, UMR 7648, Laboratoire de Physique des Plasmas, F-75005, Paris, France*
[4]*T/ICT4D, ICTP, International Centre for Theoretical Physics, StradaCostiera, 11, I-34151 Trieste Italy*
[5]*LAB-STICC, UMR 6285, Institut Mines-Telecom Atlantique, CS 83818, 29288 Brest Cédex 3, France*
[6]*Electronic Navigation Research Institute, National Institute of Maritime, Port and Aviation Technology, 7-42-23 Jindaiji-Higashi, Chofu, Tokyo 182-0012, Japan*

Received 21 June 2021; Received in revised form 06 August 2021; Accepted 05 November 2021

ABSTRACT

This paper presents the variations of the rate of change of Total Electron Content (TEC) index (ROTI), characterizing the occurrence of ionospheric plasma irregularities over Vietnam and neighboring countries in the Southeast Asian region using the continuous GPS data during the 2008-2018 period. The results showed that the occurrence of strong ROTI in all stations is maximum in equinox months March/April and September/October and depends on solar activity. The ROTI is weak during periods of low solar activity and strong during periods of high solar activity. There is an asymmetry between the two equinoxes. During maximum and declining phases of 2014-2016, occurrence rates in March equinox are larger than in September equinox, but during the descending period of 2010-2011, the occurrence rates in September equinox at almost all stations are larger than in March equinox. The correlation coefficients between the monthly occurrence rate of irregularities and the F10.7 solar index at the stations in the equatorward EIA crest region are higher than at those in the magnetic equatorial and the poleward EIA crest regions. The irregularity occurrence is high in the pre-midnight sector, maximum between 2000 LT to 2200 LT. The maximum irregularity occurrence is located around 4-5° degrees in latitude equator-ward away from the anomaly crests.

Keywords: GPS continuous data, TEC, ROTI, ionospheric irregularities, Southeast Asian region.

1. Introduction

Plasma instabilities generate the ionospheric irregularities in the ionosphere, and the electron density fluctuates randomly due to complex dynamic processes in the ionosphere. The irregularities in the ionosphere are associated with phenomena

*Corresponding author, Email: lhminhigp@gmail.com

such as sporadic E, spread F, plasma bubbles, or traveling ionosphere disturbances (TIDs). The equatorial plasma bubbles are generated by the Rayleigh-Taylor instability (Kelley, 2009 and references therein). After sunset, the F layer rises quickly under the influence of the $\vec{E} \wedge \vec{B}$ drift. The increase of the eastward electric field before its reversal, known as the pre-reversal enhancement (PRE), makes a favorable condition for Rayleigh-Taylor instability. These irregularities extent along geomagnetic field lines to higher latitudes and often reach the equatorial ionization anomaly (EIA) crest (Kelley and McClure, 1981; Ossakow, 1981). The plasma bubbles are observed to tilt westward using GPS data (Valladares et al., 2004; D'ujanga et al., 2013; Abadi et al., 2014) and reproduced by numerical models (e.g., Zalesak et al., 1982; Yokohama, 2017). A further controlling factor of the generation of equatorial ionospheric irregularities is the orientation of the solar terminator to the geomagnetic field lines (Tsunoda, 1985). In general, plasma bubbles frequently occur when the solar terminator is parallel to the geomagnetic field. A plume-like irregular structure was found in a range-time-intensity diagram by using the data from incoherent scattering radar. It was then proposed that the irregularities are produced as low-density 'plasma bubbles' at the bottom side of the ionosphere, and bubbles can easily reach even much more than 1000km (Woodman and LaHoz, 1976). The seasonal variability of the occurrence frequency of ionosphere irregularities in longitude has been studied using various satellite observations (Maruyama & Matuura, 1984; Burke et al., 2004). The plasma bubble occurrence has various temporal variations, such as day-to-day, seasonal, solar activity variabilities (Abdu, 2019; Smith and Heelis, 2017; Sahai et al., 2000; Huang et al., 2002). The TEC depletions often accompany the ionospheric irregularities with durations ranging from 5 to 25 minutes and magnitudes from 5 to 15 TEC units which affect the positional accuracy of the GPS by 1 to 3 m (Rama Rao et al., 2006). The characteristics of scintillation occurrences in low latitude around the EIA crest over Indonesia were studied in detail (Abadi et al., 2014). The authors reported that the scintillations occur in the post-sunset period (18:00-01:00LT) during the equinox months, which can be ascribed plasma bubbles. They were enhanced as solar activity increased from 2009 to 2011. Tran et al. (2017) showed that, over the Vietnam region, the scintillation activity is maximum during equinox months in the 2006-2014 period and depends on solar activity. The distribution of scintillation occurrences is dominant during the pre-midnight hours around the northern crest of EIA, from the 15°N to 20°N geographic latitudes with a maximum at about 16°N. Le Huy et al. (2016b) studied TEC variations and ionospheric irregularities during the magnetic storm in March 2015. Using continuous GPS observations in the Southeast Asian region, they showed that the ionospheric scintillations appeared strongly when the magnetic activity index Ap was less than several tens of nanoteslas. The ionospheric scintillations mainly appeared in the equatorial ionization anomaly region, with the maximum occurrence frequency being a few degrees in latitude equator-ward away from the anomaly crest.

The observational GPS technique allows the study of ionospheric irregularities. Pi et al. (1997) have defined a rate of TEC change index (ROTI), based on the standard deviation of the rate of change of total electron content (TEC) over a 5-min period to monitor the ionospheric irregularities from the GPS phase fluctuations. Since plasma bubbles can cause TEC fluctuations when the satellite beacon crosses the density depletions, Rama Rao et al. (2006) found that the TEC depletion can reach 15 TEC units. Beach & Kintner (1999) reported that the small-scale fluctuation of

TEC with a 5-minute period has a larger amplitude inside of plasma bubbles, while outside of the plasma bubbles, the amplitude is smaller. So, the ground-based GPS receivers provide a useful tool to detect ionospheric small fluctuations. This paper used GPS data to study the occurrence characteristics of ionospheric irregularities (scintillations) over Vietnam and adjacent regions during the 2008-2018 period, which covers one solar cycle. The second section presents data and calculation methods, the third one describes the results, and section 4 presents some conclusions of our research work.

2. Data and calculation method

We used the data recorded by GPS receivers in Vietnam and the Southeast Asian region. The geographical coordinates and magnetic latitudes are listed in Table 1 and present in Fig. 1. The data from some stations of the International GNSS Service (IGS): CMUM, CUSV, and CPNM in Thailand, ANMG in Malaysia, NTUS in Singapore, BAKO, and JOG2 in Indonesia, and XMIS in Australia are also used.

The slant total electron content (STEC) is determined by the carrier phase measurements (Le Huy et al., 2016b; Tam Dao et al., 2020; and references in the papers):

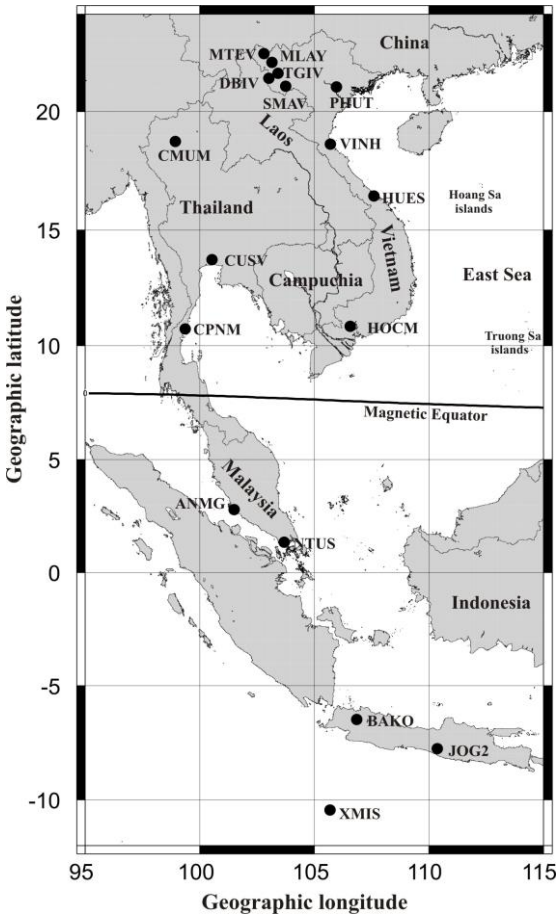

Figure 1. The distribution of GPS receivers in Vietnam and adjacent region

$$STEC = \frac{1}{40.3}\frac{f_1^2 f_2^2}{f_1^2 - f_2^2}\left[\left(L_{1j}^i - L_{2j}^i\right) + \left(b_\phi^i + b_{\phi j}\right) - \left(\lambda_1 N_{1j}^i - \lambda_2 N_{2j}^i\right)\right] = STEC_\phi + const_j^i \quad (1)$$

where i and j indices are the satellite i and the receiver j, respectively; L_1 and L_2 are phase measurements in GPS frequencies f_1 and f_2; b is instrument bias for satellite or for receiver; λ is wavelength; N is phase cycle-ambiguity. In (1) we note the STEC without the bias terms

$$STEC_\phi = \frac{1}{40.3}\frac{f_1^2 f_2^2}{f_1^2 - f_2^2}\left(L_{1j}^i - L_{2j}^i\right) \quad (2) \text{ and}$$

$$const_j^i = \frac{1}{40.3}\frac{f_1^2 f_2^2}{f_1^2 - f_2^2}\left[\left(b_\phi^i + b_{\phi j}\right) - \left(\lambda_1 N_{1j}^i - \lambda_2 N_{2j}^i\right)\right] \quad (3)$$

for each receiver-satellite pair.

One defines the pseudo-ranges STEC without the bias terms

$$STEC_p = \frac{1}{40.3}\frac{f_1^2 f_2^2}{f_1^2 - f_2^2}\left(p_{1j}^i - p_{2j}^i\right) \quad (4)$$

Carrano & Groves (2009) showed that $STEC_p$ is usually dispersed due to thermal noise and multipath therefore an imprecise observable, the quantity $STEC_\phi$ is determined precisely but suffers from jumps due to the cycle slip, and these jumps are estimated by

comparison between $STEC_\phi$ and $STEC_p$ approximated by the fourth-degree polynomial on each satellite track for only data points above 20° elevation.

To obtain the absolute TEC, we did not calculate the constant for each pair of receiver-satellite individually. Instead, we followed Komjathy et al. (2005) to use a global TEC model to evaluate instrument bias at any place on the globe. The vertical TEC (VTEC) from the global TEC model (GIM/CODG model) calculated at the sub-ionospheric point corresponding to the receiver-satellite pair at the observation time t_k is converted to STEC and compared with the corrected STECϕ at the same time to obtain $const_j^i(t_k)$. The daily constant $const_j^i$ is then calculated as the median value of all the values $const_j^i(t_k)$ on the day for each satellite. At last STEC values are converted into the vertical TEC (VTEC) using the single layer model (Klobuchar, 1986).

The rate of change of the total electron content (ROT) is computed by:

$$ROT = \frac{STEC_\phi(t+\delta t) - STEC_\phi(\delta t)}{\delta t} \quad (5)$$

where δt=30s, and ROT in TECu/min. To identify the ionospheric irregularity, the standard deviation of ROT is computed for each 5 min time interval. This value is called rate of TEC change index (ROTI) (Pi et al., 1997) and calculated as follows:

$$ROTI = \sqrt{\langle ROT^2 \rangle - \langle ROT \rangle^2} \quad (6)$$

Table 1. GPS stations in Vietnam and Southeast Asian region

No	Station	Geographical coordinate		Magnetic latitude	Instrument	Observation period
		Longitude	Latitude			
1	MTEV	102.80719	22.38719	15.92	NETRS	12/2009- 07/2018
2	MLAY	103.15385	22.04187	15.54	NETRS	01/2012- 12/2018
3	DBIV	103.01829	21.38992	14.84	NETRS	11/2009- 12/2018
4	TGIV	103.41803	21.59225	15.06	NETRS	11/2009- 12/2018
5	SMAV	103.74971	21.05629	14.49	NETRS	06/2010- 07/218
6	PHUT	105.95872	21.02938	14.49	GSV4004	02/2009- 12/2018
7	VINH	105.69659	18.64999	11.91	CORS5700	09/2011- 05/2018
10	CMUM	98.93238	18.76088	11.61	IGS station	01/2014- 12/2018
8	HUES	107.59265	16.45919	9.58	GSV4004	01/2006- 07/2013
13	CUSV	100.53392	13.73591	6.43	IGS station	05/2008- 12/2018
9	HOCM	106.55979	10.84857	3.47	GSV4004	05/2005- 08/2014
11	CPNM	99.37438	10.72465	2.80	IGS station	10/2015- 04/2018
12	ANMG	101.50660	2.78465	-5.73	IGS station	02/2014- 12/2018
14	NTUS	103.67996	1.34580	-7.05	IGS station	01/2008- 12/2018
15	BAKO	106.84891	-6.49106	-15.52	IGS station	01/2008- 12/2018
16	JOG2	110.37246	-7.73638	-16.75	IGS station	01/2013- 12/2018
17	XMIS	105.68350	-10.44996	-19.99	IGS station	01/2008-12/2018

Following the study by Nishioka et al. (2008), we used the difference between daytime and nighttime ROTI values to determine the occurrence of ionospheric irregularity events. There were three steps to identify the ionosphere irregularity events for one day at any station, as follows:

(1) Calculating the average of ROTI values from 1200 UT to 1900 UT (1900-0200 LT) (the most disturbed period), called R_{ev}.

(2) Calculating average of ROTI values during 3 hours from the noon, i.e during 0500-0800 UT (1200-1500 LT) (when VTEC is maximum), called R_{day}.

(3) Difference, $\Delta R = R_{ev}$-R_{day}, is used as an index of ionospheric irregularity activity for

one day at one station. Nishioka et al. (2008) selected value of 0.075 TECu/min as a threshold to determine ionospheric irregularity day. Fig. 2 presents variation of R_{ev}-R_{day} at PHUT in 2011. The variation of R_{ev}-R_{day} has two peaks in March/April and September/October. In Fig. 2, we can see most of R_{ev}-R_{day} values are between -0.03 TECu/min and +0.03 TECu/min. The R_{ev}-R_{day} values change within ±0.03 TECu/min could be due to the thermal noise which was not related to ionospheric disturbance because we see the values in this range on every months of the year (Fig.2), the fact could not belong to the ionospheric physical phenomena in consideration. Larger values of R_{ev}-R_{day} which exceed +0.03 TECu/min could be caused by ionospheric irregularities. To identify certainly ionospheric irregularity events, we add 0.01 TECu/min to 0.03 TECu/min of R_{ev}-R_{day} values to exclude TEC variations which are not generated by ionosphere irregularities. In this study we selected the threshold of R_{ev}-R_{day} of 0.04 TECu/min to define the irregularities day.

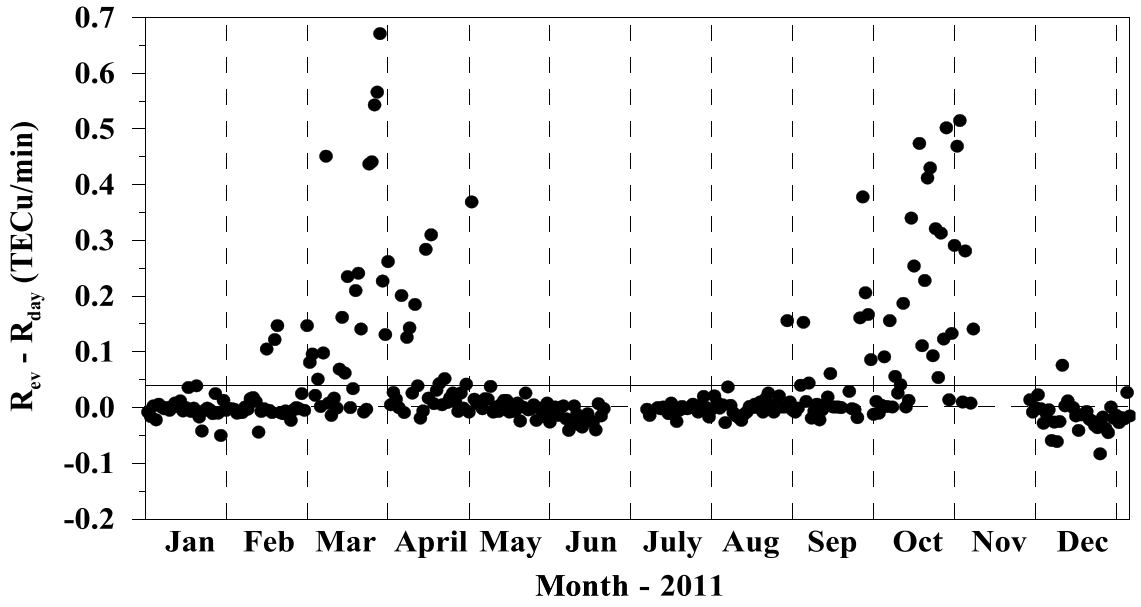

Figure 2.The variation R_{ev}-R_{day} at PHUT in 2011. R_{ev}-R_{day} values are presented by filled circles. The horizontal lines show 0.00 TECu/min and 0.04 TECu/min. The horizontal line at 0.04 TECu/min indicates the threshold for detection of ionospheric irregularity day

3. Results and discussion

3.1. TEC variation and Rate of TEC change Index

TEC was derived every 30 seconds from GPS data at all stations. When ionospheric irregularity occurs, TEC fluctuates rapidly. Examples of the diurnal TEC variations with and without ionospheric fluctuations observed at PHUT station on 2 January 2015 and 15 February 2015 are shown in Figs. 3a and 3b, respectively. The horizontal axis is in Universal Time (UT), and the vertical axis is VTEC in the TEC unit (1 TECu=10^{16} e/m^2). Figs. 3a and 3b show that daily VTEC value is high in the daytime and low in the nighttime. In Fig. 3b, we observe intense TEC fluctuations after sunset around 1200 UT (1900 LT). They are caused by a large fluctuation of the ionospheric electron density.

We also observed that the value of ROTI is low and constant during the daytime in these two days. ROTI is weak on 2 January 2015, while it is large in the post-sunset period from 1200 UT to 1900 UT (1900-0200 LT) on 15 February 2015. The large value of ROTI corresponds to a sharp fluctuation of VTEC. Therefore, ROTI was used to identify the occurrence of ionospheric scintillations using the ground-based TEC data.

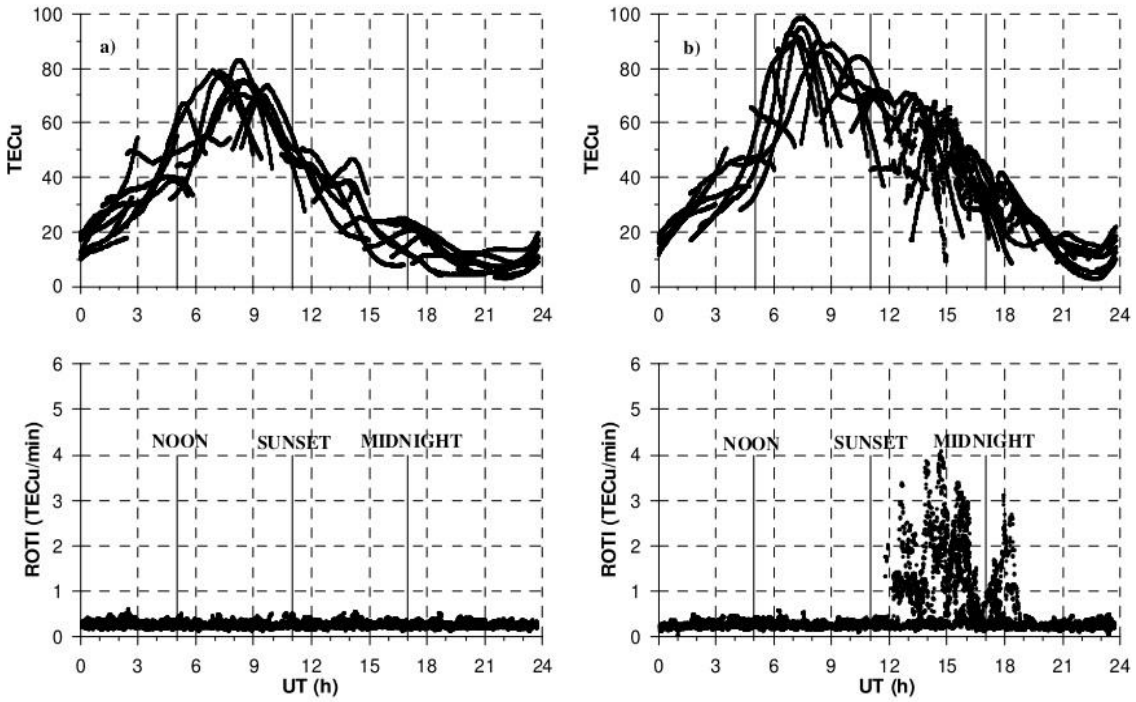

Figure 3. Daily variation of TEC and ROTI measured at PHUT on (a) 2 January 2015 and (b) 15 February 2015. (top) TEC values for all satellites, (bottom) ROTI values for all satellites calculated from the TEC data. The three solid lines correspond to noontime, sunset time and midnight time at 400 km altitude at the PHUT station

3.2. The occurrence rate of ionospheric irregularities

After calculating daily ΔR, we calculated monthly occurrence rates of ionospheric irregularities by taking the ratio of disturbance days to the observation days in one month at each station. Figs. 4 and 5 show that occurrence rates of ionospheric irregularities in all stations are maximum in equinox months March/April and September/October. This result is in good agreement with the previous studies based on different techniques in periods of high and low solar activity such as in American longitudes (Abdu et al., 2000), in Peru (Fejer et al., 1999), and in Brasil (Sahai et al., 2000). Tran et al. (2017) analyzed the amplitude scintillations (determined by S4 index) for the period 2006-2014 using GPS data at PHUT, HUES, and HOCM stations in Vietnam and found that the scintillation was maximum during equinox months and minimum during summer and winter months.

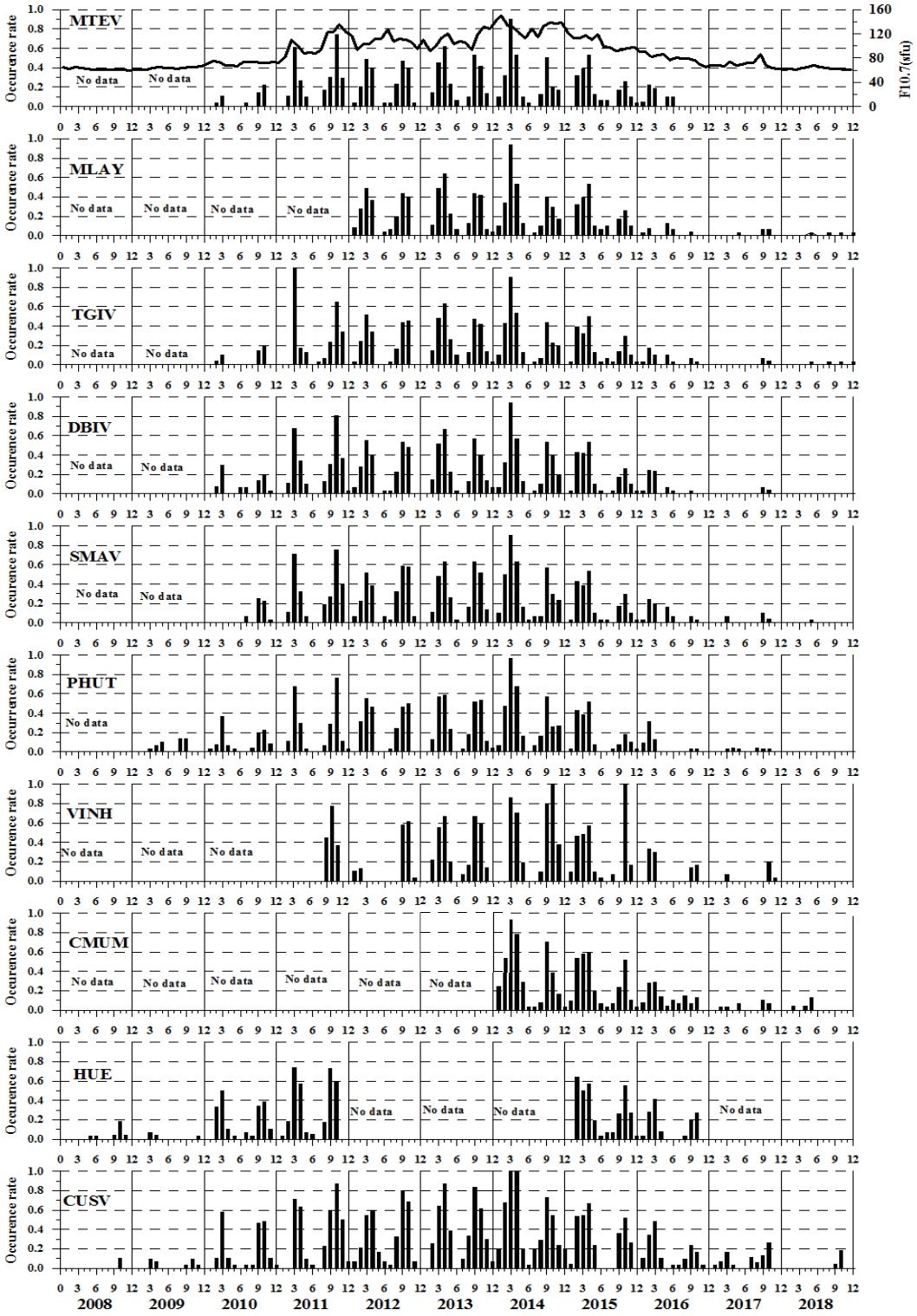

Figure 4. Monthly occurrence rates of ionospheric irregularities from 2008 to 2018 at MTEV, MLAY, TGIV, DBIV, SMAV, PHUT, VINH, CMUM, HUE, CUSV Northern stations

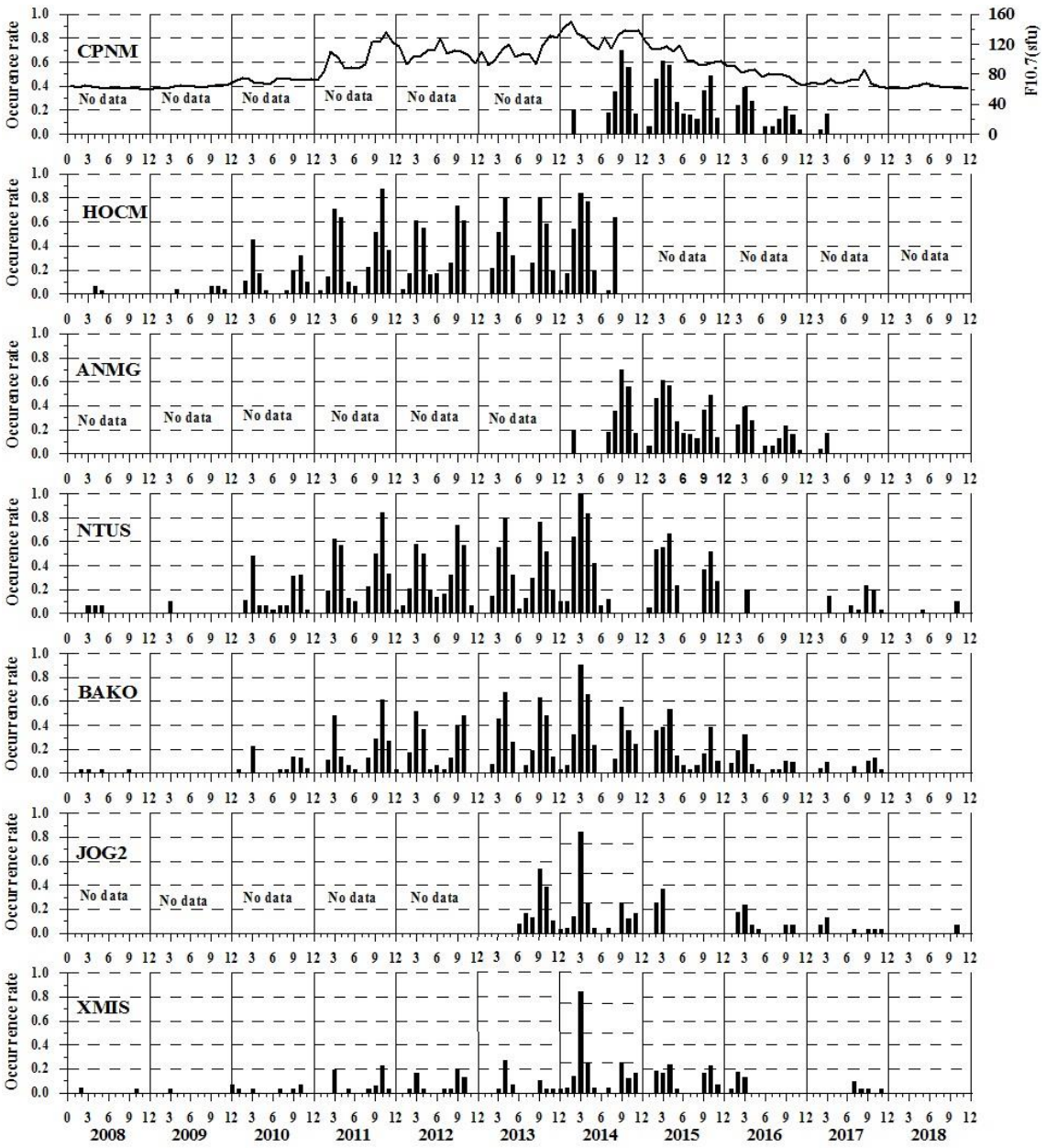

Figure 5. Monthly occurrence rates of ionospheric irregularities from 2008 to 2018 at CPNM, HOCM Northern stations and ANMG, NTUS, BAKO, JOG2, XMIS Southern ones

Many authors found the maximum occurrence of ionospheric scintillations during the equinox months in the world, such as Aarons (1993), Chandra et al. (2003), Burke et al. (2004), Nishioka et al. (2008); Abadi et al. (2014), Liu et al. (2015) for the Asian region; Huang et al. (2002), Makela et al. (2004) for the Pacific area; Wiens et al. (2006), Portillo et al. (2008), Okoh et al. (2017), Abiriga et al. (2020) for the African sector. The maximum occurrence of equatorial ionospheric irregularities in equinoxes was explained by the alignment of the magnetic meridian and the solar

terminator (Tsunoda, 1985). During the equinox, the solar terminator is aligned with the magnetic meridian, the conjugate E regions at both sides of the magnetic equator enter darkness simultaneously. The conductivity of the E region is low while the equatorial ionosphere is still raised in altitude. Thereby, the strong enhancement of the eastward electric field around sunset creates favorable conditions for generating ionosphere irregularities. We observed an asymmetry between the maxima of occurrence rates of ionospheric scintillations in March/April and September/October. In descending phase of 2014-2016, occurrence rates in March equinox were larger than in September equinox. In the increasing phase of 2010-2011, the occurrence rates in September equinox at almost all stations are larger than in March equinox. Nishioka et al. (2008) showed that in the Asia region during 2005 and 2006 (in descending phase), the occurrence rates of the plasma bubbles in March equinox were larger than in September equinox. Our observations are consistent with those results of Nishioka et al. (2008) for the Asia region.

Considering the possible control parameters, some mechanisms for explaining the seasonal variation of the occurrence rates of ionospheric irregularities (equatorial spread F and plasma bubbles) have been proposed such as: (1) the seasonal changes of the reversal time of the electric field from eastward to westward in the evening hours after sunset (Rastogi, 1980); (2) the small-scale electric fields generated in the E region can be transferred to the F region and magnetosphere along magnetic field lines due to a hemispheric asymmetry of the wind in the dynamo region (Mudrew, 1980); (3) the transequatorial component of the thermospheric wind which modifies the Pedersen conductivity integrated along the magnetic field line (Maruyama & Matuura, 1984); (4) the longitudinal gradient in integrated E region Pedersen conductivity controlled by the magnetic declination and geographic latitude of the dip equator at a given longitude (Tsunoda, 1985); (5) the east-west component of plasma drift velocity may be related to the evolution of plasma irregularities causing scintillations throughout the mechanism causing the prereversal enhancement of the eastward electric fields (Otsuka et al., 2006).

The influence of a transequatorial wind appears to depress the F layer in the lee side hemisphere and to rise it in the windward hemisphere; the asymmetric distribution of the ionization may increase in the magnetic field integrated Pedersen conductivity, which suppresses the growth of the Rayleigh-Taylor instability and the ionospheric irregularity activity. Using data from two vertical ionospheric probes near the magnetic conjugate points at Chiang Mai, Thailand (18.8°N, 98.8°E; 13.0° magnetic latitude) and Kototabang, Indonesia (0.2°S, 100.3°E; -10.0° magnetic latitude) for the September equinox, 2004 and March equinox 2005, Maruyama et al. (2009) found that the amplitude of the meridional wind in September equinox in 2004 is larger than in March equinox in 2005, and the occurrence probability of equatorial irregularities is lower in September 2004 than in March 2005. These observations are consistent with the hypothesis that the transequatorial wind suppresses the Rayleigh-Taylor instability, decreasing the nighttime ionospheric irregularities (Maruyama & Matuura, 1984). This is clear evidence for the meridional wind control of the ionospheric irregularities. Maruyama et al. (2009) calculated the thermospheric wind pattern for 2004-2005 in the descending phase of solar activity and confirmed the equinoctial asymmetry of the ionospheric irregularity occurrence in the descending phase. The pattern of the thermospheric wind in the ascending phase needs further investigations. Recently, Hu et al. (2020) measured the

statistical characteristics of the appearance of plasma plumes based on VHF radar observations at Sanya during the equinoxes for the period 2011-2016. They found the opposite patterns in the equinoctial asymmetry of the plasma plumes in 2011 (in the solar ascending phase) and in 2015 (descending phase), which corresponded well with those in the sunset increases of h'F in 2011 and 2015. These observations suggested that the equinoctial asymmetry of plume occurrence in 2011 and 2015 could be caused mainly by the asymmetric sunset F layer height, which controls the growth rate of R-T instability.

Figs. 4 and 5 also represent the monthly variation of the F10.7 solar index from 2008 to 2018. We observed that the ionospheric irregularities depend on solar activity. The monthly occurrence rates of irregularities are strong in the years of the high solar sunspot (2012-2014). In 2008, 2009, and 2018, in minimum solar activity, irregularity rates are very small with no irregularities recorded in some stations such as PHUT, VINH, MTEV, SMAV, XMIS, and BAKO.

To estimate the effect of solar activity on the ionospheric irregularities, we calculated the correlation between the monthly occurrence rate of irregularities and the monthly F10.7 solar index for some stations. The results were listed in Table 2 and presented in Fig. 6.

We see that the correlation coefficients could be divided into three groups with different value ranges: (1) for the stations CPNM and ANMG near the magnetic equator, they are 0.51, 0.52, respectively; (2) for the stations at the crest regions as VINH, CMUM, CUSV and HOCM in northern hemisphere and BAKO, NTUS in the southern one, they are in the range of 0.56÷0.61; (3) for the stations outside EIA crest regions as MTEV, MLAY, TGIV in the northern hemisphere and JOG2, XMIS in the southern one, they are in the range of 0.39÷0.49. Therefore, the correlation coefficients between the monthly occurrence rate of irregularities and the monthly F10.7 solar index at the stations near the equatorward EIA crest region are higher than at the magnetic equatorial and the poleward EIA crest regions.

Table 2.The correlation coefficient between the monthly occurrence rate of the ionospheric irregularities and monthly F10.7 solar index

No	Station	Magnetic latitude	During period	Correlation coefficient
1	MTEV	15.92	2010-2018	0.39
2	MLAY	15.54	2012-2018	0.49
3	TGIV	15.06	2010-2018	0.39
4	DBIV	14.84	2010-2018	0.51
5	SMAV	14.49	2010-2018	0.49
6	PHUT	14.49	2009-2018	0.50
7	VINH	11.91	2011-2018	0.58
8	CMUM	11.61	2014-2018	0.61
9	CUSV	6.43	2008-2018	0.57
10	HOCM	3.47	2008-2014	0.61
11	CPNM	2.8	2015-2018	0.51
12	ANMG	-5.73	2014-2018	0.52
13	NTUS	-7.05	2008-2018	0.59
14	BAKO	-15.52	2008-2018	0.56
15	JOG2	-16.75	2013-2018	0.47
16	XMIS	-19.99	2008-2018	0.44

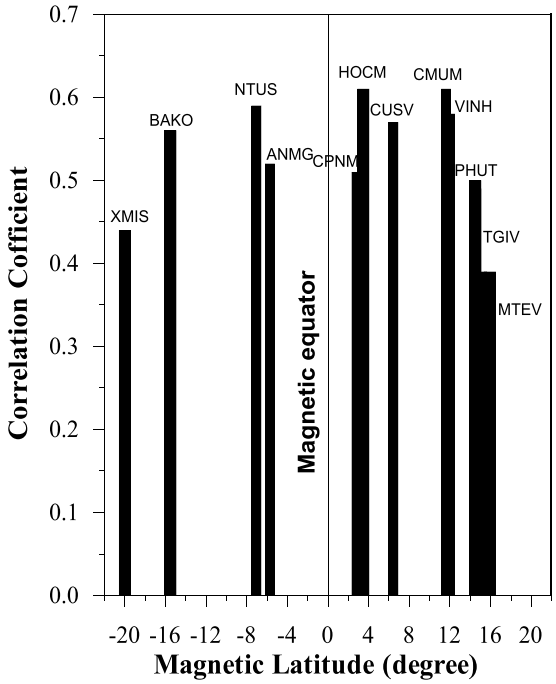

Figure 6. The correlation coefficient between monthly occurrence rate of ionospheric irregularities and monthly F10.7 solar index at different stations

Previous studies showed that the ionospheric irregularities at EIA region are primarily associated with equatorial plasma bubbles (EPBs) (Rama Rao et al., 2006; Saito et al., 2008; Abadi et al., 2014; Bhattacharyya et al., 2014). EPBs are TEC depletions in which the bottom side F region becomes unstable at the magnetic equator after sunset. These EPBs often cause scintillation in the GPS signal. They are generated by Rayleigh-Taylor plasma instability. Some previous studies (Basu et al., 1978; Kelley & McClure, 1981; Mendillo & Baumgardner, 1982; Cervera & Thomas, 2006; Rama Rao et al., 2006) found that EPBs extend from the magnetic equator to the crest of the EIA region. The regions around the crests of EIA have the ambient electron density to be higher than at the dip equatorial region. Beniguel et al. (2009) and Abadi et al. (2014) reported that strong scintillations concentrate in EIA crest regions. Since the intensity of amplitude scintillation is proportional to the background electron density, strong scintillations are expected at the EIA crest region where the electron density is high (Abadi et al., 2015). Valladares et al. (2004) showed that the scintillations reach maximum at almost lower latitudes than the boundary of the EIA crest at the American longitudinal sector. Therefore, strong scintillations concentrate near equatorward EIA crest regions such as VINH, CMUM, CUSV, HOCM, BAKO, and NTUS. Hence the correlation coefficients between the monthly occurrence rate of irregularities and the monthly F10.7 solar index at these stations are higher than at other ones. These correlations are worse than the correlation between the amplitude of the TEC at the two crests with a sunspot number that is 0.90 (as reported by Le Huy et al., 2016a). This can be explained as the ionospheric electron density is primarily impacted by solar activity, while disturbance activity depends on the complicated ionospheric, magnetic, and solar conditions.

In addition, ionospheric irregularities at the EIA region are caused by medium-scale traveling ionosphere disturbances (MSTIDs). Imposing an MSTID as an externally-imposed traveling-wave electric field on the SAMI3/ESF model post-sunset ionosphere, Krall et al. (2011) showed that the coupling between the MSTID at low- to mid-latitudes and the equatorial F layer leads to the growth of equatorial plasma bubbles. Lakshmi Narayanan et al. (2014) showed that the boundary of the MSTIDs appearance might exist around the equatorial ionization anomaly crest, and the equatorial ionization anomaly is involved in preventing the movement of MSTIDs to reach lower and equatorial latitudes. Lakshmi Narayanan et al. (2014) also reported that the midnight pressure bulge (MPB) associates with MSTID and plays a role in suppressing MSTID moving to lower

latitudes. Taori et al. (2015) reported that MSTID at the low latitude and EPB at the equator occur simultaneously over India. The authors discussed that observed MSTID could be seeded to trigger forming EPB in low-equatorial latitudes, and this EPB propagates upward at low latitudes. Hisao et al. (2018) observed EPB events accompanying the presence of MSTIDs without conditions favorable for F-layer uplifting over the South American continent. The study also concluded that MSTIDs could be one seeding source to generate EPBs. Le Huy et al. (2016b) observed MSTIDs during the magnetic storm in March 2015 in the Southeast Asia region, generated in the EIA crest at Northern hemisphere after sunset and propagates equatorward with a speed of about 210 m/s. Therefore, MSTIDs moving toward the equator as one of the sources of EPB forming may also cause high ionospheric irregularity activities at stations near equatorward EIA crest regions. Recently, using the data from the GPS receiver network in Japan for 22 years from 1998 to 2019, Otsuka et al. (2021) revealed the solar activity dependence of the MSTIDs at mid-latitudes. They found that the nighttime MSTID activity and occurrence rate increased with descending solar activity (higher at solstice and in low solar activity). Subsequently, this solar activity dependence of the MSTIDs may degrade the correlation of the nighttime ionospheric irregularity with the solar activity. This should be further investigated by distinguishing events either EPB type or MSTID type. The triggering of EPBs by MSTIDs is an interesting topic but difficult to study with the data shown in this study.

3.3. The latitudinal and time distribution of ionospheric irregularities

To estimate the distribution of nighttime ionospheric irregularities in latitude and time, we mapped ROTI ≥ 0.5 TECu/min values (Ma & Maruyama, 2006) in time versus latitude at all GPS stations in Vietnam and adjacent region during 2008-2018. These results are shown in Fig. 7. The figure is divided into a grid with one pixel (0.5 h×0.5°) corresponding to universal time (UT=LT-7) and geographic latitude for all days. We observe the following features: (1) most of the ionospheric irregularities occur after sunset until pre-midnight (from 1800 to 2400 LT), (2) the irregularity activity is maximum at about from 2030 to 2200 LT, (3) there are very few irregularities during post-midnight hours. We also observe the concentration of the ionospheric irregularities at geographic latitudes about from 15° to 22°N (8°-15° magnetic latitudes). In 2008-2009 and 2017-2018, solar activity is so weak that the distribution of ionospheric irregularities is not clear. In addition, in the Southern hemisphere, there are few stations. Consequently, the distribution of ionospheric scintillations in the Southern hemisphere is less clear than in the Northern one. Fig. 7 shows yearly mean TEC maps in time vs latitude in the Southeast Asian area during 2008- 2018, with a contour interval of 5 TECu. We found that yearly mean TEC values have two maximum crests on the two sides of the magnetic equator. The northern crest is observed near the latitude of 20°-22°N, i.e. in the Northern part of Vietnam and the southern crest is observed in the latitude 5°-7°S. Le Huy et al. (2014) showed that the location of the monthly northern crest of the EIA in the Vietnam region during the 2006-2011 period varies between 17°N and 22°N geographic latitudes (about 10°-15°N magnetic latitudes). Therefore, we can conclude that the ionospheric scintillations occur more around the northern crest of the EIA than at the magnetic equator. Some previous studies on ionospheric disturbance using ionospheric scintillation data also found the concentration of scintillation around the EIA (Valladares et al., 2004; Rama Rao et al., 2006).

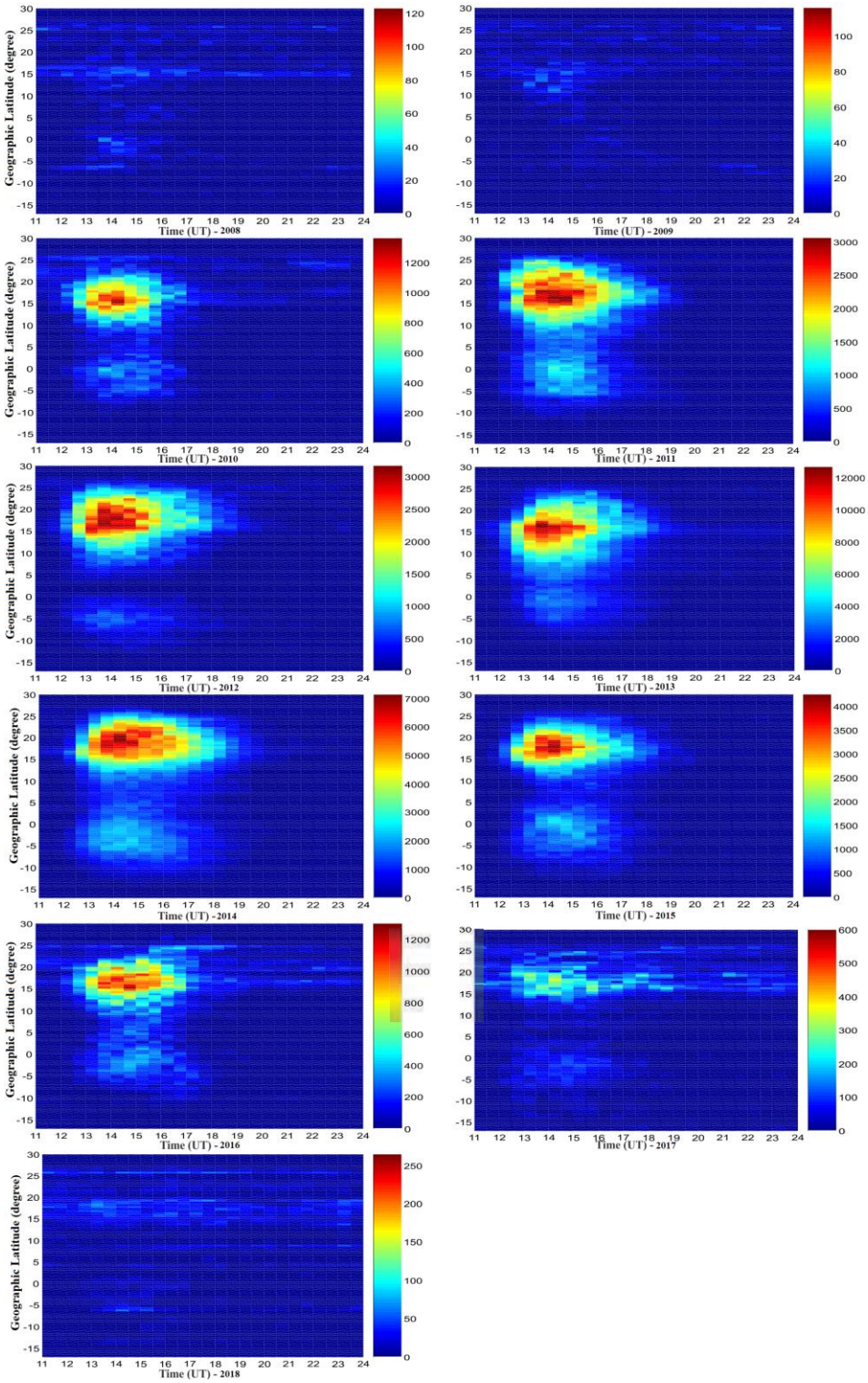

Figure 7. Map in latitude versus universal time of ROTI ≥ 0.5 TECu/min for the period 2008-2018 in Vietnam and adjacent region

Fig. 8 also shows that during the years of low solar activity (from 2008-2009 and 2017-2018), both anomaly crests' magnitude and latitudinal extension are low, together with low ambient electron densities, so irregularity activity is weak. During strong solar activity (from 2010-2016), the high ambient electron density leads to high irregularity activity. At low latitudes, arranging these irregularities through the magnetic field lines depends on the altitude reached by the irregularities. When these irregularities are mapped down to the equatorial anomaly crest region, where the ambient electron density is higher compared to the electron density in the equatorial region, it results in stronger irregularities in the region near the anomaly crest than the equatorial region (Bhattacharyya et al., 2014; Tran et al., 2017). Therefore, it is reasonable to observe the high activity of ionospheric irregularities, which occur more near the crests of the EIA than in the equatorial region.

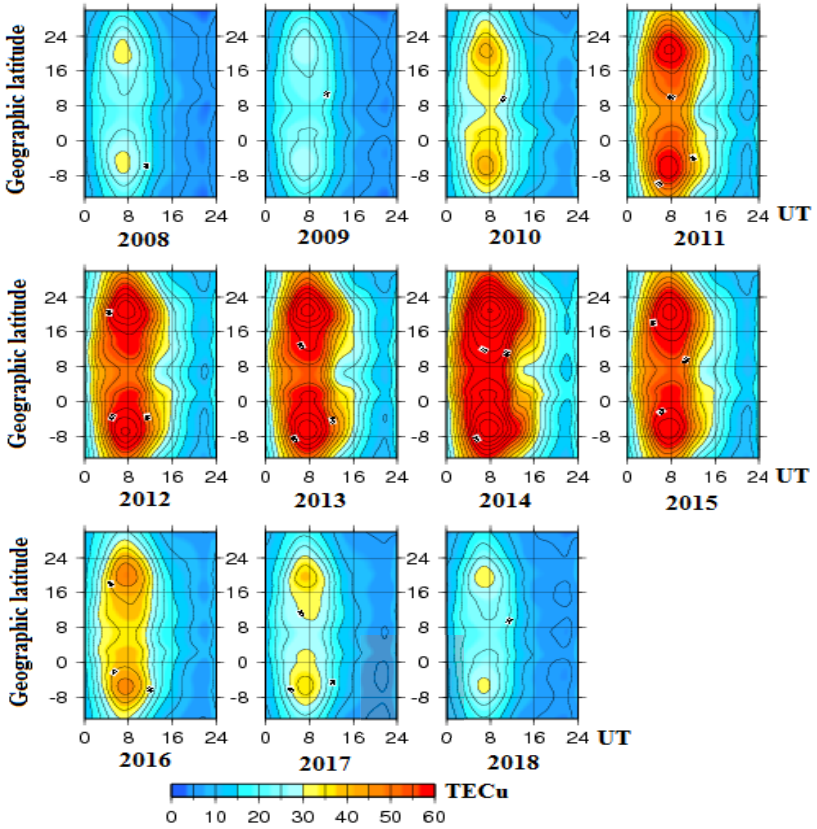

Figure 8. Time and latitudinal yearly mean TEC maps in the Southeast Asian area for the 2008-2018 period. Contour interval: 5 TECu

However, Fig. 9, which illustrates the latitudinal distribution of irregularities (ROTI ≥0.5), shows that ionospheric irregularities are more concentrated near the EIA crest than at the magnetic equator, but the peak of occurrence does not coincide with the EIA crest. Figure 10 presents the geographic latitude of EIA crests and the geographic latitude of maximum irregularity occurrence in both hemispheres from 2010 to 2017, the maximum of irregularities in both hemispheres are almost in lower latitudes other than EIA crests (the maximum irregularities occurrence location is of about 4-5° degrees in latitude equator-ward away from the anomaly crests).

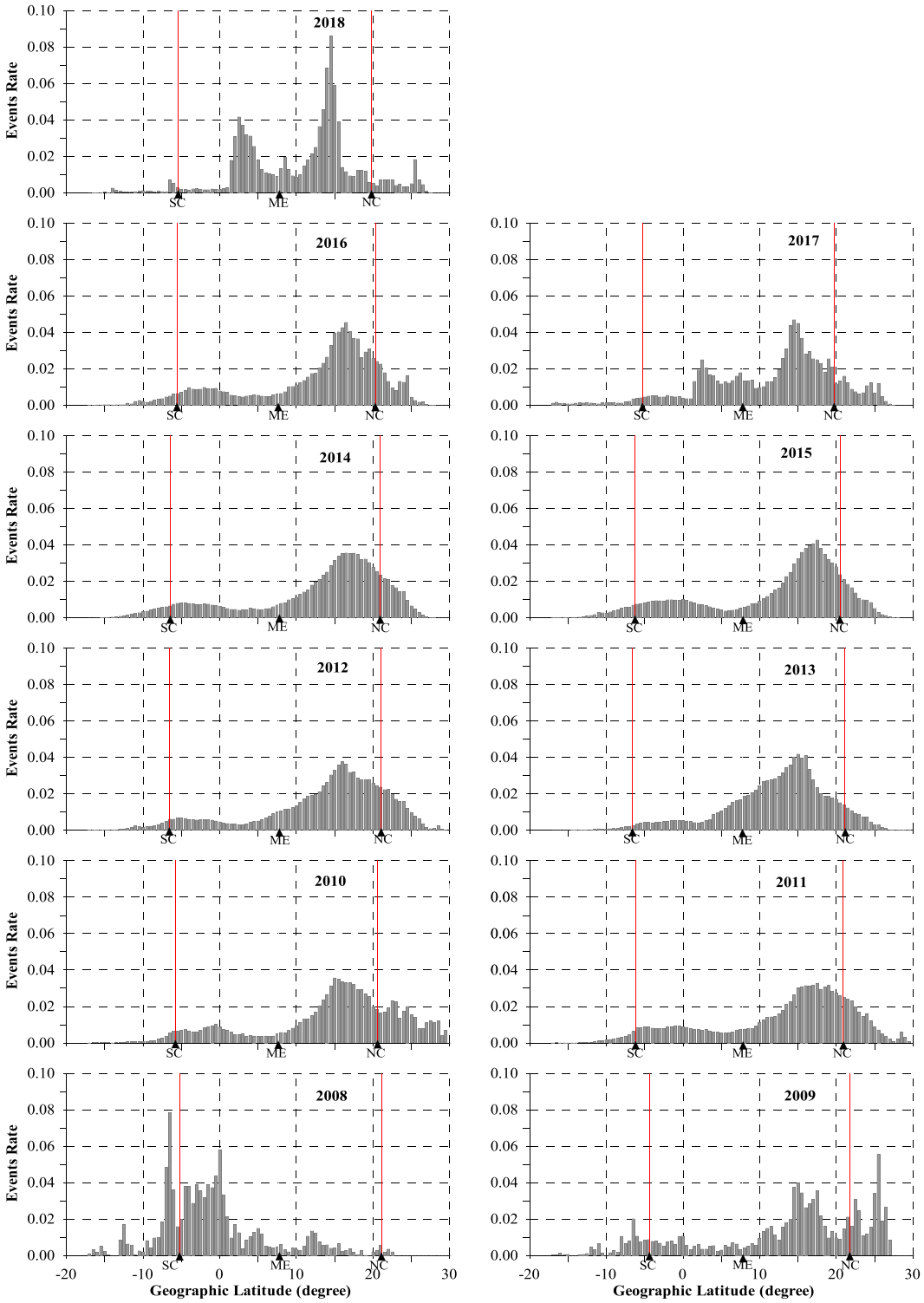

*Figure 9.*Statistics of ionospheric scintillations (ROTI≥0.5) along geographic latitude during the period 2008-2018. ME: magnetic equatorial; SC: southern crest; NC: northern crest

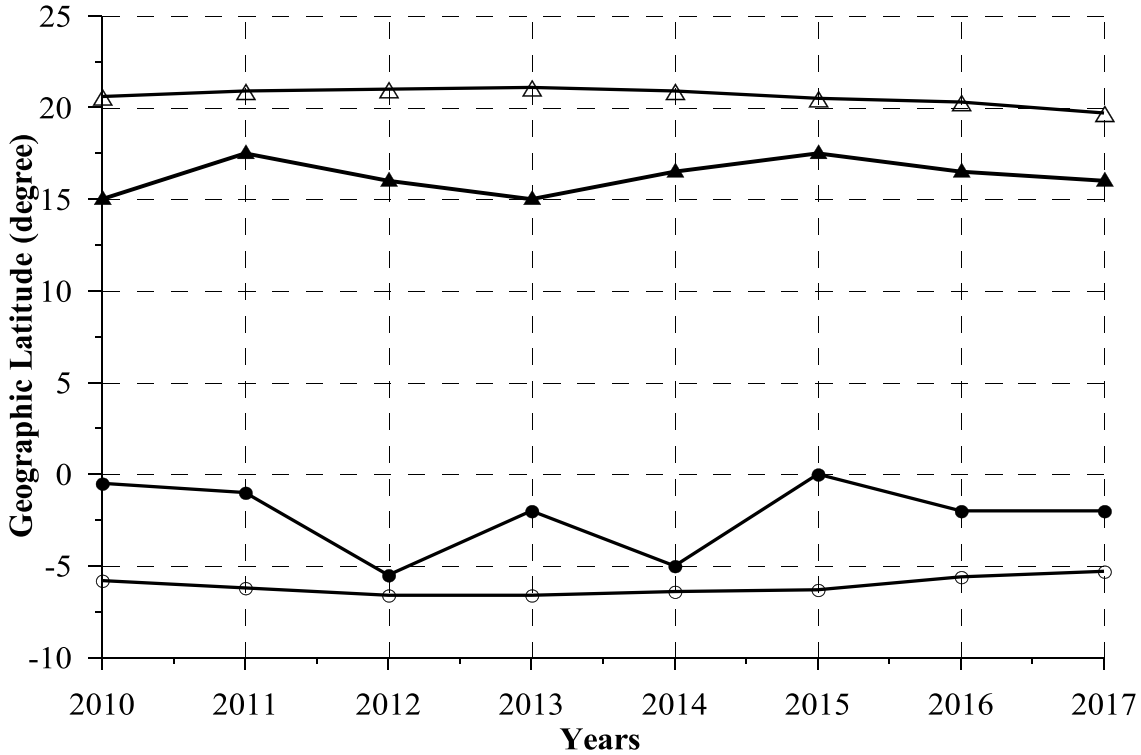

Figure 10. The geographic latitude of EIA crests and the geographic latitude of position where the ionospheric irregularity occurrence is maximum from 2010 to 2017. Triangle black line and circle black line represent the latitude of northern and southern EIA crests, respectively. Filled triangle black line and filled circle black line represent the geographic latitude of position where the ionospheric scintillation occurrence is maximum at the Northern and Southern hemispheres, respectively

Moraes et al. (2018) analyzed the GPS data from four different stations over Brazillian territory (one close to the geomagnetic equator, two near the southern crest of EIA, and one on the poleward side of the EIA crest). They mentioned the high scintillation occurrence near the EIA crest. Our new findings were the detailed relationship between the EIA crests (TEC peak, Fig. 8) and ROTI peak, and the ROTI peaks were slightly equatorward of the EIA crests in the Northern and Southern hemispheres. The new finding can be explained as follows: (1) ROTI should be higher when the background density is higher because irregularity is usually perturbation concerning the background density and proportional to the one, i.e., it is around EIA crests; (2) Plasma bubbles which are the primary source of irregularity in the low latitude region develop from the magnetic equatorial area, and do not all reach EIA crests, i.e., the occurrence of source events is higher in the magnetic equatorial region; (3) In the combination of the two effects, background density and source event occurrence, the occurrence of events with ROTI values higher than a certain threshold would maximize equatorward of the EIA crests. In addition, we can say that this is useful to develop a scintillation occurrence model to estimate GNSS applications' performance.

4. Conclusions

By using continuous GPS data networks in Vietnam and adjacent regions during 2008-

2018, we investigated the occurrence characteristics of ROTI and VTEC. We derived monthly occurrence rates and distribution of irregularity in latitude vs time.

The occurrence rates of irregularities in all stations were maximum during equinox months March/April and September/October for all years (2008-2018) and depend on solar activity. We also observed to have an asymmetry of the occurrence rate ROTI between two equinoxes. In the maximum and declining phases of 2014-2016, occurrence rates in March equinox are larger than in September equinox. In the increasing phase of 2010-2011, occurrence rates in September equinox are larger than in March equinox.

The correlation coefficients between the monthly occurrence rate of irregularities and the F10.7 solar index at the stations near the equatorward EIA crest region are higher than at the magnetic equatorial and the poleward EIA crest regions. The irregularities are dominant in the pre-midnight sector and maximum at about from 2030 to 2200 LT. We also observe the concentration of the irregularity activity at geographic latitudes about from 15°-22°N (8°-15° magnetic latitudes). The maximum irregularity occurrence location is almost in lower latitudes than the peak of EIA about 4-5° equator-ward. Accordingly, we could conclude that the ionospheric irregularities occur more often at the equator-ward EIA region than at the magnetic equatorial and the poleward EIA regions.

Acknowledgements

We are thankful to the anonymous referees for reviewing and helping us to improve our paper and to the IGS Community for making available GNSS data. This study has been supported by the Vietnam Academy of Science and Technology (VAST05.04/20-21, NVCC 12.02/21-21) and by the NAFOSTED under grant 105.05-2019.310.

References

Aarons J., 1993. The longitudinal morphology of equatorial F-layer irregularities relevant to their occurrence. Space Sci. Rev., 63(3-4), 209-243.

Abadi P., S. Saito, W. Srigutomo, 2014. Low-latitude scintillation occurrences around the equatorial anomaly crest over Indonesia. Ann. Geophys., 32, 7-17.

Abadi P., Y. Otsuka, T. Tsugawa, 2015. Effects of pre-reversal enhancement of E×B drift on the latitudinal extension of plasma bubble in Southeast Asia. Earth Planets Space, 67. Doi: 10.1186/s40623-015-0246-7.

Abdu M.A., 2019. Day-to-day and short-term variabilities in the equatorial plasma bubble/spread F irregularity seeding and development. Prog. Earth Planet Sci., 6, 11. https://doi.org/10.1186/s40645-019-0258-1.

Abdu M.A., J.H.A. Sobral, I.S. Batista, 2000. Equatorial spread F statistics in the American longitudes: Some problems relevant to ESF description in the IRI scheme. Adv. Space Res., 25(l), 113-124.

Abiriga F., E.B. Amabayo, R. Jurua, P.J. Cilliers, 2020. Statistical characterization of equatorial plasma bubbles over East Africa. J. Atmos. Sol.-Terr. Phys., 105197. Doi: 10.1016/j.jastp.2020.105197.

Basu S., S. Basu, J. Aarons, J.P. McClure, M.D. Cousins, 1978. On the coexistence of kilometer- and meter-scale irregularities in the nighttime equatorial F region. J. Geophys. Res., 83(A9), 4219-4226.

Beach T.L., P.M. Kintner, 1999. Simultaneous global positioning system observations of equatorial scintillations and total electron content fluctuation. J. Geophys. Res. 104(A10), 22553-22565, https://10.1029/1999jA00220.

Beniguel Y., V. Romano, L. Alfonsi, M. Aquino, A. Bourdillon, P. Cannon, G. de Franceschi, S. Dubey, B. Forte, V. Gherm, N. Jakowski, M. Materassi, T. Noack, M. Pozoga, N. Rogers, P. Spalla, H. J. Strangeways, E.M. Warrington, A. Wernik, V. Wilken, N. Zernov, 2009. Ionospheric scintillation monitoring and modeling. Annals Geophys., 52(3-4), 391-416.

Bhattacharyya A., B. Kakad, S. Sripathi, K. Jeeva, K.U. Nair, 2014. Development of intermediate scale structure near the peak of the F region within an

equatorial plasma bubble. J. Geophys. Res., 119, 3066-3076.

Burke W.J., L.C. Gentile, C. Y. Huang, C.E. Valladares, and S. Y. Su, 2004. Longitudinal variability of equatorial plasma bubbles observed by DMSP and ROCSAT-1. J. Geophys. Res., 109, A12301. Doi: 10.1029/2004JA010583.

Carrano C., K. Groves, 2009. Ionospheric data processing and analysis. Workshop on Satellite Navigation Science and Technology for Africa, The Abdus Salam ICTP. Trieste. Italy.

Cervera M.A., R.M. Thomas, 2006. Latitudinal and temporal variation of equatorial ionospheric irregularities determined from GPS scintillation observations. Ann. Geophys., 24(12), 3329-3341.

Chandra H., S. Sharma, M.A. Abdu, I.S. Batista, 2003. Spread-F at anomaly crest regions in the Indian and American longitudes. Adv. Space Res., 31(3), 717-727. Doi: 10.1016/s027.

D'ujanga F.M., P. Baki, J.O. Olwendo, B.F. Twinamasiko, 2013. Total electron content of the ionosphere at two stations in East Africa during the 24-25 October 2011 geomagnetic storm. Adv. Space Res., 51, 712-721.

Fejer B.G., L. Scherlies, E.R. de Paula, 1999. Effects of the vertical plasma drift velocity on the generation and evolution of equatorial spread F. J. Geophys. Res., 104(A9), 19859-19869.

Hisao T., M.W. Cristiano, A. O. B. F. Cosme, B. Diego, A. A. Mangalathayil, O. Yuichi, S. Kazuo, 2018. Equatorial plasma bubble seeding by MSTIDs in the ionosphere. Progress Earth Planet. Sci., 5, 3, https://doi.org/10.1186/s40645-018-0189-2.

Hu L., X. Zhao, W. Sun, Z. Wu, J. Zheng, H. Xie, Z. Huang, B. Cing, G. Li, 2020. Statistical characteristics and correlation of low latitude F region bottom-type irregularity layers and plasma plumes over Sanya. J. Geophys. Res.: Space Phys., https:/doi.org/10.1029/2020JA027855.

Huang C.Y., W.J. Burke, J.S. Machuzak, L.C. Gentile, P.J. Sultan, 2002. Equatorial plasma bubbles observed by DMSP satellites during a full solar cycle: Toward a global climatology. J. Geophys. Res: Space Physics, 107(A12), SIA 7-1-SIA 7-10. Doi: 10.1029/2002ja009452.

Kelley M., 2009. The Earth's Ionosphere: Plasma Physics and Electrodynamics, 96, second ed. eBook ISBN: 9780080916576. Academic Press. Elsevier, New-York.

Kelley M.C., J.P. McClure, 1981. Equatorial spread-F: A review of recent experimental results. J. Atmos. Terr. Phys., 43(5), 427- 435.

Klobuchar J., 1986. Design and characteristics of the GPS ionospheric time-delay algorithm for single frequency users, in: Proceedings of PLAN'86-Position Location and Navigation Symposium. Las Vegas. Nevada, 280-286, 4-7, November.

Komjathy A., L. Sparks, B.D. Wilson, A.J. Mannucci, 2005. Automated daily processing of more than 1000 ground-based GPS receivers for studying intense ionospheric storms. Radio Sci., 40, RS6006, http://dx.doi.org/10.1029/2005RS003279.

Krall J., J.D. Huba, S.L. Ossakow, G. Joyce, J.J. Makela, E.S. Miller, M.C. Kelley, 2011. Modeling of equatorial plasma bubbles triggered by non-equatrial traveling ionosphericdistrubances. Geophys. Res. Lett., 38, L08103. Doi: 10.1029/2011GL046890.

Lakshmi Narayanan V., K. Shiokawa, Y. Otsuka, S. Saito, 2014. Airglow observations of nighttime medium-scale traveling ionospheric disturbances from Yonaguni: Statistical characteristics and low-latitude limit. J. Geophys. Res., 119(11), 9268-9282. Doi: 10.1002/2014ja020368.

Le Huy M., C. Amory-Mazaudier, R. Fleury, A. Bourdillon, P. Lassudrie Duchesne, Tran Thi L., Nguyen Chien T., Nguyen Ha T., P. Vila, 2014. Time variations of the total electron content in the Southeast Asian equatorial ionization anomaly for the period 2006-2011. Adv. Space Res., 54, 355-368.

Le Huy Minh, Tran Thi Lan, C. Amory Mazaudier, R. Fleury, A. Bourdillon, J. Hu, Vu Tuan Hung, Nguyen Chien Thang, Le Truong Thanh, Nguyen Ha Thanh, 2016a. Continuous GPS network in Vietnam and results of study on the total electron content in the South East Asian region. Vietnam J. Earth Sci., 38(2), 153-165.

Le Huy Minh, Tran Thi Lan, R. Fleury, C. Amory Mazaudier, Le Truong Thanh, Nguyen Chien Thang, Nguyen Ha Thanh, 2016b. TEC variations and

ionospheric disturbances during the magnetic storm in March 2015 observed from continuous GPS data in the Southeast Asia region. Vietnam J. Earth Sci., 38(3) 267-285.

Liu K., G. Li, B. Ning, 2015. Statistical characteristics of low-latitude ionospheric scintillation over China. Adv. Space Res., 55(5), 1356-1365. Doi: 10.1016/j.asr.2014.12.001.

Ma G., T. Maruyama, 2006. A super bubble detected by dense GPS network at east Asian longitudes. Geophys., Res. Lett., 33, L21103. Doi: 10.1029/2003JA009931.

Makela J.J., B.M. Ledvina, M.C. Kelley, 2004. Analysis of the seasonal variations of equatorial plasma bubble occurrence observed from Haleakala, Hawaii. Ann. Geophys., 22(9), 3109-3121. Doi: 10.5194/angeo-22-3109.

Maruyama T., N. Matuura, 1984. Longitudinal variability of annual changes in activity of equatorial spread F and plasma bubbles. J. Geophys. Res., 89(A12), 10.903-10.912, https://doi.org/10.1029/jA039iA12p10903.

Maruyama T., S. Saito, M. Kawamura, K. Nozaki, J. Krall and J. D. Huba, 2009. Equinoctial asymmetry of a low-latitude ionosphere-thermosphere system and equatorial irregularities: evidence for meridional wind control. Ann. Geophys., 27, 2027-2034.

Mendillo M., J. Baumgardner, 1982. Airglow characteristics of equatorial plasma depletions. J. Geophys. Res., 87(A9), 7641. Doi: 10.1029/ja087ia09p07641.

Moraes A. de O., B.C. Vani, E. Costa, J. Sousasantos, M.A. Abdu, F. Rodrigues, Y.C. Gladek, C.B.A. de Oliveira, J.F.G. Monico, 2018. Ionospheric scintillation fading coefficients for the GPS L1, L2 anf L5 frequencies, Radio Sci., 53, 1165-1174. Doi: 10.1029/2018RS006653.

Muldrew D.B., 1980. The formation of ducts and spread F and the initiation of bubbles by field-aligned currents. J. Geophys. Res., 85(A2), 613-625.

Nishioka M., A. Saito, T. Tsugawa, 2008. Occurrence characteristics of plasma bubble derived from global ground-based GPS receiver networks. J. Geophys. Res., 113, A05301. Doi: 10.1029/2007JA012605.

Okoh D., B. Rabiu, K. Shiokawa, Y. Otsuka, B. Segun, E. Falayi, R. Kaka, 2017. First Study on the Occurrence Frequency of Equatorial Plasma Bubbles over West Africa Using an All-Sky Airglow Imager and GNSS Receivers. J. Geophys Res: Space Physics, 122(12). Doi: 10.1002/2017JA024602.

Ossakow S.L., 1981. Spread- F theories - A review. J. Atmos. Terr. Phys., 43, 437-443.

Otsuka Y., A. Shinbori, T. Tsugawa, M. Nishioka, 2021. Solar activity dependence of medium-scale traveling ionospheric disturbances using GPS receivers in Japan. Earth Planets Space, 73, 22. Doi: 10.1186/s40623-020-01353-5.

Otsuka Y., K. Shiokawa, T. Ogawa, 2006. Equatorial ionospheric scintillations and zonal irregularities drifts observed with closely-spaced GPS receivers in Indonesia. J. Meteor. Soc. Jpn., 84A, 343-351.

Pi X., A.J. Mannucci, U.J. Lindqwister, C.M. Ho, 1997. Monitoring of global ionospheric irregularities using the worldwide GPS network. Geophys. Res. Lett., 24(18), 2283-2286.

Portillo A., M. Herraiz, S.M. Radicella, L. Ciraolo, 2008. Equatorial plasma bubbles studied using African slant total electron content observations. J. Atmos. Sol.-Terr. Phys., 70(6), 907-917. Doi: 10.1016/j.jastp.2007.05.019.

Rama Rao P.V.S., S. Gopi Krishna, K. Niranjan, D.S.V.V.D. Prasad, 2006. Study of spatial and temporal characteristics of L-band scintillation over the Indian low latitude region and their possible effects on GPS navigation. Ann. Geophys., 24, 1567-1580.

Rastogi R.G., 1980. Seasonal variation of equatorial spread F in the American and Indian zones. J. Geophys. Res., 85(A2), 722-726.

Sahai Y., P.R. Fagundes, J.A. Bittencourt, 2000. Transequatorial F-region ionospheric plasma bubbles: solar cycle effects. J. Atmos. Terr. Phys., 62(15), 1377-1383. Doi: 10.1016/s1364-6826(00)00179-6.

Saito S., S. Fukao, M. Yamamoto, Y. Otsuka, T. Maruyama, 2008. Decay of 3-m-scale ionospheric irregularities associated with a plasma bubble observed with the Equatorial Atmosphere Radar. J. Geophys. Res: Space Physics, 113, A11318. Doi: 10.1029/2008JA013118.

Smith J., R.A. Heelis, 2017. Equatorial plasma bubbles: Variations of occurrence and spatial scale in local time, longitude, season, and solar activity. J. Geophy. Res.: space Physics, 122, 5743-5755., Doi: 10.1002/2017JA024128.

Tam Dao, Minh Le Huy, Brett Carter, Que Le, Thanh Thuy Trinh, Bao Ngoc Phan, 2020. New observations of the total electron content and ionospheric scintillations over Ho Chi Minh City. Vietnam J. Earth Sci., 42(4), 320-333. Doi: 10.15625/0866-7187/42/4/15281.

Taori A., N. Parihar, R. Ghodpage, N. Dashora, S. Sripathi, E.A. Kherani, P. T. Patil, 2015. Probing the possible trigger mechanisms of an equatorial plasma bubble event based on multi-station optical data. J. Geophys Res: Space Physics, 120(10), 8835-8847.

Tran Thi Lan, Le Huy Minh, C. Amory-Mazaudier, R. Fleury, 2017. Climatology of ionospheric scintillation over the Vietnam low-latitude region for the period 2006-2014. Adv. Space. Res., 60(8), 1657-1669. Doi: 10.1016/j.asr.2017.05.005.

Tsunoda R.T., 1985. Control of the seasonal and longitudinal occurrence of equatorial scintillations by the longitudinal gradient in integrated E region Pedersen conductivity. J. Geophys. Res., 90(A1), 447-456.

Valladares C.E., J. Villalobos, R. Sheehan, M.P. Hagan, 2004. Latitudinal extension of low latitude scintillations measured with a network of GPS receivers. Ann. Geophys., 22, 3155-3175.

Wiens R.H., B.M. Ledvina, P.M. Kintner, M. Afewerki, Z. Mulugheta, 2006. Equatorial plasma bubbles in the ionosphere over Eritrea: occurrence and drift speed. Ann. Geophys., 24, 1443-1453.

Woodman R.F., C. La Hoz 1976. Radar observations of F region equatorial irregularities. J. Geophys. Res., 81(31), 5447-5466. Doi: 10.1029/ja081i031p05447.

Yokoyama T., 2017. A review on the numerical simulation of equatorial plasma bubbles toward scintillation evaluation and forecasting. Progress Earth Planet. Sci., 4, 37. Doi: 10.1186/s40645-017-0153-6.

Zalesak S.T., S.L. Ossakow and P.K. Chaturvedi, 1982. Nonlinear equtatorial spread F: The effect of neutral winds and background pedersen conductivity. J. Geophys. Res., 87(A1), 151-166, https://doi.org/10.1029/jA087iA01o00151.